Contribution of Mechanical and Fluid Stresses to the Magnitude of In-stent Restenosis at the Level of Individual Stent Struts

Brandis K. Keller,[1] Claudia M. Amatruda,[2,3] D. Rodney Hose,[2,3] Julian Gunn,[3,4] Patricia V. Lawford,[2,3] Gabriele Dubini,[1] Francesco Migliavacca,[1] and Andrew J. Narracott[2,3]

[1]Laboratory of Biological Structure Mechanics (LaBS), Department of Chemistry, Materials and Chemical Engineering 'Giulio Natta', Politecnico di Milano, Milan, Italy; [2]Medical Physics Group, Department of Cardiovascular Science, University of Sheffield, Sheffield, UK; [3]INSIGNEO Institute for in Silico Medicine, University of Sheffield, Sheffield, UK; and [4]Department of Cardiovascular Science, University of Sheffield, Sheffield, UK

(*Received 13 November 2013; accepted 18 February 2014; published online 26 February 2014*)

INTRODUCTION

Despite the improved success rates of coronary artery angioplasty with stenting for revascularisation of an occlusive atherosclerotic lesion, acute inflammation of the vessel wall and resultant in-stent restenosis (ISR) may result in a need for further clinical intervention in the stented lesion. Re-intervention is required in around 20% of clinical cases where bare metal stents are used. This figure is reduced to less than 10% for drug-eluting stents (DES),[41] leading to increased clinical use of DES.[40] The reaction of the vessel wall to the stent can be described as a wound healing response consisting of four phases: thrombosis, inflammation, cellular proliferation, and vessel remodelling.[12] Excessive cellular proliferation, resulting in neointimal hyperplasia (NIH), leads to the formation of an extensive neo-intima within the stented region for some patients. NIH has been linked with both non-physiological stresses applied to the vascular wall[31] and with modification of the fluid dynamic environment within the vessel.[21] Numerous studies have shown that mechanical forces imposed by the device during deployment and the resulting radial compression of the artery wall by the stent struts lead to a localised biological response,[16,44] whilst fluid dynamic effects, including spatial and temporal alterations in wall shear stress (*WSS*) on the stented arterial wall,[24,31] have been shown to affect the migration of endothelial cells during the initial healing stages.[8,15] Suppression of the response to stent implantation using pharmaceutical agents has demonstrated improvements in treatment, as demonstrated with DES. However, improved understanding of the relationship between the modifications to

Address correspondence to Andrew J. Narracott, Medical Physics Group, Department of Cardiovascular Science, University of Sheffield, Sheffield, UK. Electronic mail: a.j.narracott@sheffield.ac.uk

Brandis K. Keller and Claudia M Amatruda shared first authorship.

arterial biomechanics which take place following stent implantation and the resulting response of the tissue of the arterial wall has the potential to further improve existing stent designs and inform development of novel approaches, such as bioresorbable stents.[14]

Understandably, implantation of a stent creates a substantial change in the mechanical environment of the artery. The first damage is the trauma provoked by balloon dilation during stent placement. Contact between the stent struts and the arterial wall results in local injury, of varying degrees of severity.[16] The middle layer of the artery wall (tunica media) is comprised of vascular smooth muscle cells (VSMCs). In a healthy vessel these serve to maintain vessel structure and tone, through a series of mechano-transduction processes[45] but, following arterial injury, VSMCs proliferate, migrate towards the lumen and produce extracellular matrix.[1] The detail of cellular response leading to ISR has been studied in both humans and animals, with porcine coronary artery models providing important information on the relationships between arterial injury and biological response.[4]

The change in the mechanical environment of the vessel wall following stenting has been investigated using finite element techniques to analyse different stresses, proposed as measures injury caused by the stent struts, namely; radial compression[3,26] and von Mises stress under each stent strut[2] and high tensile stress due to stent deployment.[44] Changes in cyclic deformation have also been proposed as contributors to ISR supported by evidence from *in vitro* experiments in a mock vascular phantom.[9] Decreased cyclic strain due to the high stiffness in the stented region was associated with increased VSMC proliferation and decreased apoptosis under these conditions.

Regions of onset and progression of vascular disease have been shown to correlate with vascular regions exposed to a $WSS < 0.4$ Pa,[27] with the contributing biological mechanisms including the promotion of shear-induced inflammatory cell aggregation and slow endothelial regrowth following injury.[15,22,30] Both low time-averaged *WSS* and high oscillatory shear index (*OSI*) have been associated with biological responses relevant to ISR.[7,18] Time-varying shear stress within the typical physiological range has been shown to decrease expression of the gene for endothelin-1 mRNA, reducing proliferative stimuli.[28] Regions of the vessel wall subject to elevated values of *OSI* (>0.2) have been associated with an increased risk of NIH as a result of the removal of this protective mechanism.[19,34] These fluid dynamic effects occur following stent deployment due to the high stiffness of the stent relative to the vessel, inducing regions of retrograde or oscillating flow which have been linked with increased incidence of NIH.[43] Local geometry can have significant effect and hence, when investigating the links between fluid dynamic factors and NIH, it is important that CFD simulations are carried out using geometries that are representative of the coronary artery geometry post-stenting.[25]

Whilst computational studies are becoming increasingly sophisticated, with the use of patient-specific images for the construction of structural and/or fluid domains,[32,36] the relative roles of solid and fluid mechanics in the process of ISR remain to be determined. Previous studies have compared *in vivo* measurements with symmetrically expanded stent models in order to gain averaged information about the role of mechanical and fluid dynamic contributions,[5] but analysis of the localised correlation between the geometry of the stent and the local effects of these stimuli acting on the wall was not undertaken. In cases where data documenting the degree of ISR is available, characterisation of local stimuli arising from vascular solid and fluid mechanics under consistent conditions may help to determine the relative importance of these stimuli.

This paper describes a method to analyse the localisation of both structural and fluid dynamic stresses, using the finite element method (FEM) and computational fluid dynamics (CFD) respectively, using *in vivo* 3D stent geometry obtained from a porcine model of ISR in combination with an idealised vessel wall domain. The volumetric micro-CT data provides the *in vivo* deployed stent geometry; the structural and fluid stresses acting on the computational vessel wall are then interpreted at the level of individual struts for comparison with the degree of ISR observed in histological sections of the explanted stented vessel.

MATERIALS AND METHODS

This study reports computational analysis based on experimental data obtained from a porcine restenosis model. All animal experiments were performed in accordance with the UK Animals (Scientific Procedures) Act, 1986. Analysis of the micro-CT and histology data used for this study has been previously reported[33] with only fluid dynamics stimuli considered for a partial section of the fluid domain, without the consideration of a physiological vessel curvature. The experimental methods have been reported previously[33] and are reviewed here for completeness.

A stainless steel BiodivYsio balloon expandable stent (Biocompatibles Ltd., UK) was implanted into a healthy porcine right coronary artery (RCA), using a balloon-to-artery ratio of 1.4:1. This specific deployment ratio was carefully selected in order to induce

neointimal growth without inflicting excessive injury to the vessel. The animal was sacrificed, and the stented vessel harvested, at 14 days post-deployment. The vessel was then fixed in 10% buffered formaldehyde and embedded in methacrylate resin. The embedded vessel was imaged with high resolution micro-Computed Tomography (micro-CT) (Skyscan, Belgium) and the 3D geometry of the stent struts was reconstructed into a 3D surface mesh. Following micro-CT scanning the embedded vessel was sectioned for histomorphometric evaluation. To facilitate comparison between the experimental data and the results of numerical analysis the axial location of histology sections within the 3D micro-CT geometry were determined by visual inspection of strut morphology.[33]

Computational models of the solid and fluid mechanics within the stented artery are described below, both of these numerical models used the deployed stent geometry, obtained from volumetric micro-CT, as the starting point in combination with idealised models of the porcine right coronary artery assuming a cylindrical geometry of constant radius and wall-thickness. Distributions of solid and fluid stimuli derived from numerical simulations were compared with the biological response measured in seven transverse histological sections taken along the length of the stented region. ISR was quantified from histology at each cross-section by measurement of the neointimal thickness (*NIT*) at individual strut locations. *NIT* per-strut was calculated as the radial distance between the stent strut and the lumen margin (Fig. 1).

FEM Computational Model

Structural simulations of wall mechanics were undertaken using an individual model, of length 7.5 mm, centred at the axial location of each of the seven histological sections where measures of *NIT* were obtained. The benefit of this sampling approach over a full 3D model was that this allowed greater local mesh refinement in the region of interest. A coronary artery model was created within ANSYS Mechanical APDL v14.0 (ANSYS Inc., Canonsburg, PA) with an initial diameter of 2.8 mm (the luminal diameter of the right porcine coronary artery obtained *in vivo* from angiography prior to stenting) and a wall thickness of 0.1 mm based on a ratio ($h/2r = 0.04$) of wall thickness (h) to vessel diameter ($2r$).[35] The stress-free diameter of the FEA model corresponds to the diameter measured from angiography, as such the pressure in the FEA analysis represents pressure above mean physiological pressure. The arterial properties were represented by a hyperelastic material model with a third-order strain energy density function[13]:

$$U = 0.04 \cdot (I_1 - 3) + 0.003 \cdot (I_2 - 3)^2 + 0.085 \cdot (I_2 - 3)^3$$

where I_1 and I_2 are the first and the second invariants of the Cauchy–Green tensor. The resulting mesh comprised 19200 solid elements (SOLID185) for the vessel, 98102 target elements (TARGE170) for the stent and 6400 contact elements (CONTA173) for the inner layer of the vessel that would interact with the stent (Fig. 2a). Mesh sensitivity tests were undertaken to ensure results did not change significantly with further mesh refinement. The number of elements used in the 3 directions were: 160 around the vessel circumference, 3 through the vessel thickness and 40 in the axial direction. Elements were equally sized around the circumference and refined through thickness and along the axial direction with a ratio of 2 and 0.5 respectively between the element size at the centre and at the edges (as shown in Fig. 2b in the axial direction). Reducing element size by a factor of two in each direction resulted in changes of less than 2, 8 and 5% of the maximum compressive force (*CF*), respectively. This choice of mesh density also resulted in a good element shape, which allowed the simulations to converge without issues due to poor element aspect ratio. Sensitivity of the results to both model length and element type were also evaluated. Variation in the *CF* when either doubling the length of the model domain or using the higher order SOLID186 element type was of the same order as the variation observed with changes in mesh density: in both cases these effects have limited influence on the relative distribution of *CF* over the arterial wall, which determines the overall correlation with the biological response.

The stent was assumed to be rigid and constrained in all degrees of freedom. Axial motion of the vessel was constrained at the ends, while rigid body motion was suppressed by constraining the displacements in x

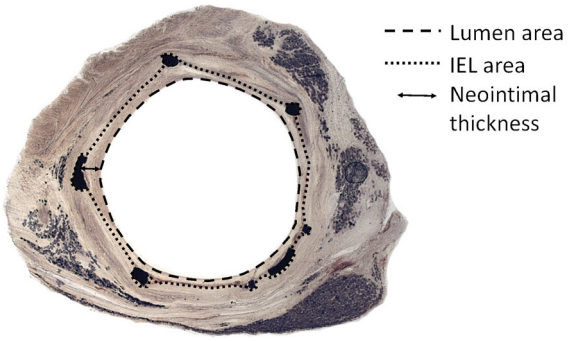

FIGURE 1. Histology slide showing the extent of NIH covering the stent struts. The coarse dashed line indicates the lumen area, the fine dashed line shows the area bounded by the internal elastic lamina (IEL). The *NIT* at each strut is defined as the distance from the stent strut to the vessel lumen.

direction at $x = 0$ and the displacements in y direction at $y = 0$ at the ends of the vessel, yet allowing free radial expansion. In the first load step, the vessel geometry was expanded using a pressure (40 kPa) of similar magnitude to that imposed during a typical angioplasty procedure, distending the vessel beyond the deployed stent diameter. In the second load step, contact was activated to capture the interaction between the stent and the inner surface of the vessel as the vessel was released onto the stent (Fig. 2c). FEM simulations were performed on a 64-bit desktop computer equipped with a 3.20 GHz quad-core processor and 16 GB RAM.

FEM Calculations for Analysis

The local compression caused by the stent strut was evaluated following stent/vessel contact. The third principal stress value, which represents the radial compression of the vessel wall (Fig. 2d), was integrated over the surface of a region local to each strut position, providing a measure of the *CF* acting on the arterial wall. The axial length of this region (0.15 mm) was constant for all segments and strut locations. The circumferential extent of the region varied with strut location and was chosen to include the contribution of each strut to the compression of the arterial wall. The compressive component was chosen from observation of the initial development of ISR, localised in the area of the stent struts in early stages of the biological response following stent implantation.

CFD Computational Model

For CFD simulations an idealised vessel of length 36 mm, radius 2.8 mm and wall thickness 0.1 mm was used to obtain the deformed state of the vessel post-stenting using an explicit methodology (ABAQUS Explicit v6.10, Dassault Systems Simulia Corp., RI, USA) as described previously in Morlacchi *et al.*[33] The surface domain of the deformed state was used to create a fluid volume mesh region using ANSYS ICEM CFD v13.0 (ANSYS Inc., Canonsburg, PA). In the present study, a 28 mm radius of curvature was chosen to represent the inlet and outlet vessel geometry (Fig. 3a) positioned according to a visible residual curvature in the micro-CT images of the stent; the centreline for the vessel was assumed to be a plane curve. The curvature ratio is defined as $\delta = a/R = 0.05$, where a is the radius of the artery inlet and R the radius of curvature. This value of curvature was based on measurements taken from 2D spline

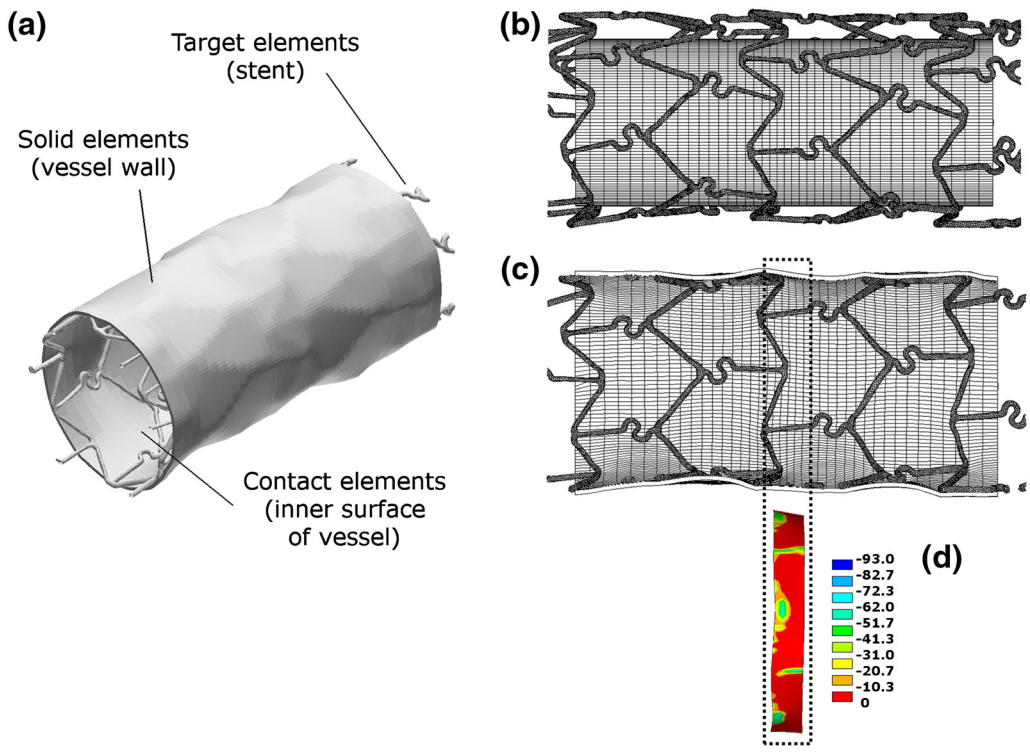

FIGURE 2. (a) Element types used in the finite element model. (b) Initial configuration of the geometry before radial expansion of the vessel wall. (c) Final configuration of the vessel geometry after expansion and subsequent release onto the stent. (d) Stress contours (kPa) on the inner surface of the vessel in the region used to compute the local force acting on the tissue corresponding to the histology data.

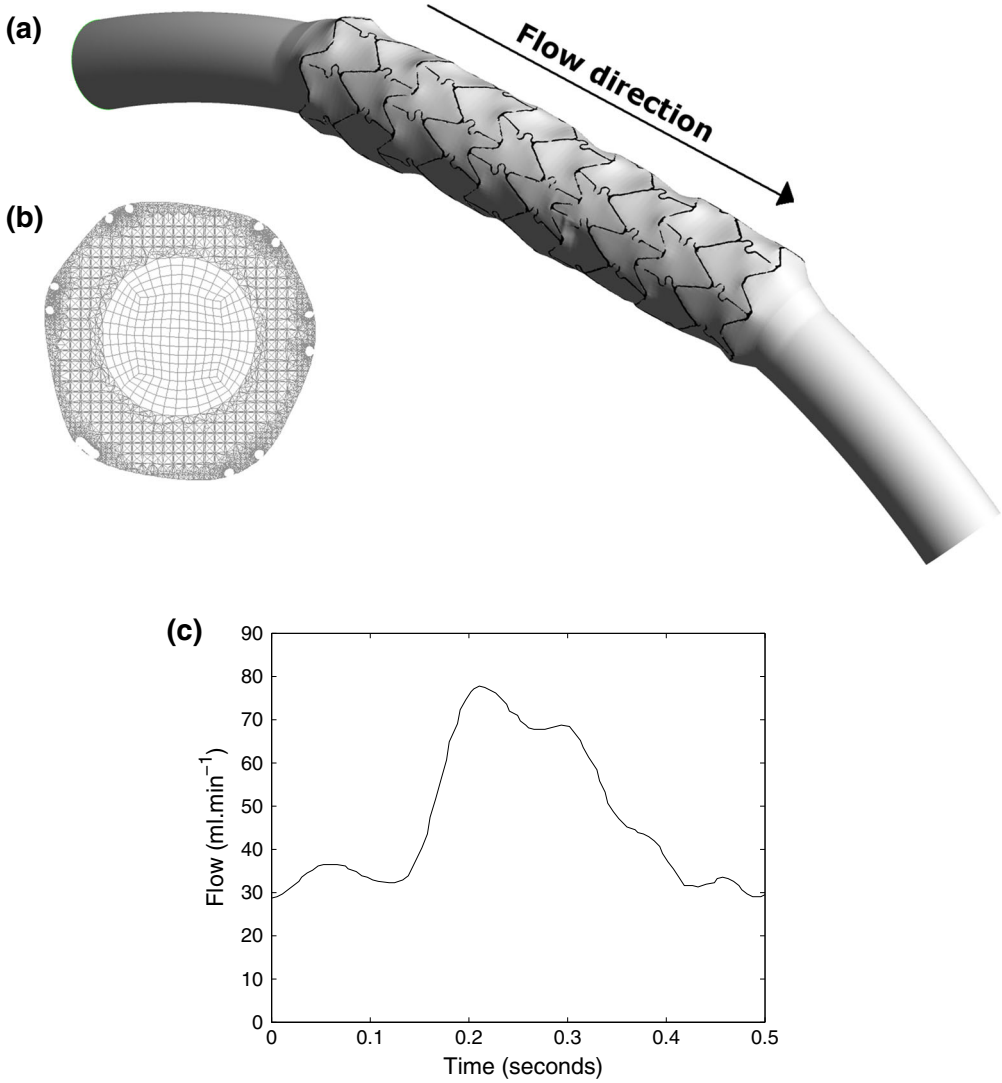

FIGURE 3. (a) Geometry used for CFD simulations. (b) Internal CFD hybrid mesh scheme. (c) Flow waveform over a single cardiac cycle for porcine right coronary artery, adapted from Huo *et al.* (with permission).

measurements on single-plane angiographic images of three similar (juvenile Yorkshire White) porcine RCA models (28.92 ± 4.06 mm) and single-plane coronary angiograms of the human RCA.[29] For simplicity, vessel torsion (out of plane curvature) was not included in the model, as the combined effect of curvature and torsion has been shown to be similar to curvature alone.[37]

The fluid domain was defined using a hybrid (combined hexahedral and Octree tetrahedral) mesh[6] shown in Fig. 3b and comprised 2974793 elements and 6206954 nodes. This mesh density was chosen following grid independence tests when the difference for the area-weighted average and percent area coverage for *WSS* fell below 1%.

Time-dependent simulations were performed using the finite-volume ANSYS FLUENT solver (v13.0). Blood was modelled as an incompressible fluid ($\rho = 1060$ kg/m^3), with non-Newtonian viscosity defined using the Carreau model with the following parameters: $\mu_\infty = 0.0035$ kg/m s, $\mu_o = 0.25$ kg/m s, $\lambda = 25.00$ s and $n = 0.25$, obtained from the literature.[38] A pulsatile flow waveform (Fig. 3c) was applied at the inlet using a parabolic velocity profile according to Huo *et al.*[17] This profile was scaled to represent the flow within a porcine RCA with an average flow rate of $Q = 47$ mL/min (mean velocity = 0.125 m/s), and cardiac cycle of 0.5 s. The geometry and inlet conditions specified above result in a maximum Reynolds number, $Re = 108.09$ justifying the assumption of laminar flow; the Dean number, $\kappa = Re\sqrt{\delta}$, was calculated to be 24.17, which is within the range for coronary flow.[20] The relative pressure on the outlet was set to 0 Pa. The artery and stent were modelled as

rigid wall boundaries with no-slip conditions. This is a reasonable assumption based on the high stiffness of the stent relative to the vessel wall.[23] The Coupled scheme was used for pressure–velocity coupling, and second-order upwind discretisation was used for the momentum transport equations. Under-relaxation factors of 0.4 for pressure and momentum and 1 for density were used. Convergence was achieved for continuity and momentum when residuals fell below 10^{-7}. The time step size was set to 0.005 s after an appropriate temporal sensitivity analysis. Simulations were performed on a desktop computer, equipped with a 3.06 GHz quad-core processor with 16 GB RAM, using 4 parallel processors.

CFD Calculations for Analysis

The time-averaged *WSS* magnitude, and *OSI* were evaluated at locations corresponding to the histological sections. *OSI* describes the degree of deviation of the *WSS* ($\vec{\tau_w}$) from its average direction during pulsatile flow and is defined as follows:

$$OSI = \frac{1}{2}\left(1 - \frac{\left|\int_0^T \vec{\tau_w} dt\right|}{\int_0^T \vec{\tau_w} dt}\right)$$

OSI was calculated using a Matlab sub-routine (MathWorks, Natick, MA, USA) and plotted using Tecplot Focus (v2, Bellevue, WA, USA) to identify regions with high *OSI*. Both haemodynamic indices were evaluated and compared with the measure of *NIT* derived from histology in the region of each stent strut (Fig. 1). Haemodynamic properties were averaged over the circumferential region local to each strut, this region extended either side of each strut to the midpoint between the strut in question and its neighbour Due to non-symmetric strut geometry and deployment, the distance between struts changes. As the response of the artery to altered haemodynamics may depend on the behaviour of cells within the region of the strut this approach accounts for variation of haemodynamics in the region of each strut. As a result, the combined measure of *CF* and averaged *WSS* accounts for effects that are focal to the strut (*CF*) and distributed within the region of the strut (averaged *WSS*).

Statistical Analysis

Linear regression was applied to the data, comparing measured *NIT* at each strut location with the computational parameters (*CF*, *WSS*, *OSI*) and reporting the corresponding coefficient of determination (R^2). The combined parameters CF/WSS and $CF \times OSI$ were compared with *NIT*, as low *WSS* and high *CF* and *OSI* are proposed to stimulate neointimal growth.

RESULTS

Four quantities were taken into consideration, one measure of biological response (*NIT*) and three numerical solution variables to represent the mechanical (*CF*) and fluid (*WSS* and *OSI*) stimuli acting on the vessel wall. Results were computed at seven locations within the stented region to provide a direct comparison with histological data at the level of individual stent struts giving a total of 53 data points throughout the stented region.

Figure 4 shows the seven histological sections (upper pane) along with the volumetric stent geometry acquired from segmentation of the microCT dataset (middle pane). The axial location of each histological section is illustrated on the segmented microCT image, providing the position at which the numerical solutions were compared with histology. Figure 4 also shows (lower pane) the contours of time-averaged *WSS* on the vessel lumen throughout the stented region for a 180° segment of the vessel.

Figure 5 shows histological data from three of the seven cross-sections shown in Fig. 4 (upper pane) along with the variation of results within each histological section. Sections were selected to illustrate the variation in *NIT* within the proximal, middle and distal regions of the stented vessel, which resulted in a percent restenosis by area of 41.8, 20.4, and 23.7%, respectively. Figures 5a and 5b and c show the histological sections together with the convention used to locate strut position in the line plots shown in Figs. 5d, 5e and 5f. Figures 5d, 5e and 5f show the variation in *NIT* (computed from histological sections), *CF* (computed by FEM analysis) and time-averaged *WSS* (computed by CFD analysis) within each section. The x axis of each plot represents the strut angular position, α, defined in Figs. 5a, 5b and 5c.

Figure 6 shows linear regression plots for mechanical stimuli, *CF*, and haemodynamic parameters, *WSS* and *OSI*, in the region of each strut plotted against the *NIT* at each strut location. The correlation between *NIT* and the combined parameters CF/WSS, $CF \times OSI$ and OSI/WSS is also presented. Values for the slope, m, intercept, b, and correlation coefficient, R^2, for each plot are reported in Table 1.

DISCUSSION

This study demonstrates the influence of realistic 3D deployed stent geometry on the structural and fluid

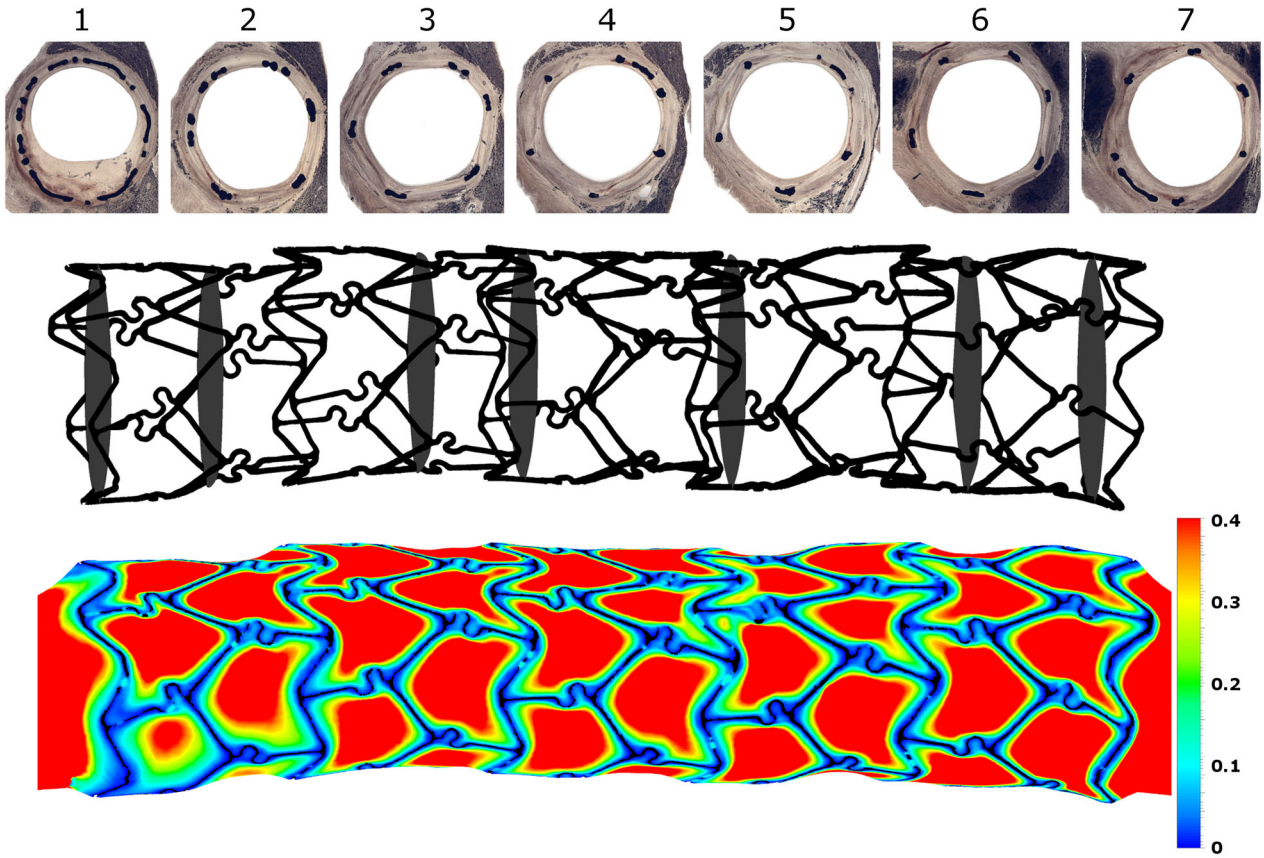

FIGURE 4. The seven histology cross-sections used for evaluation of the biological response to stent implantation (upper pane). Stent geometry from microCT segmentation, showing locations of the seven histology cross-sections (middle pane). Contour of *WSS* (Pa) throughout the stented region for a 180° section of the vessel wall (lower pane).

mechanics following stent deployment. Direct comparison between these stimuli and the biological response at the level of individual stent struts is possible through the coupling of 3D volumetric micro-CT images of stent geometry and 2D histological sections.

The FEM simulations indicate that *CF*s are higher at the proximal and distal ends of the stented region than in the central region (Figs. 5d, 5e and 5f). In the proximal region, increase in *CF* is co-located with a greater biological response, (Fig. 5d). However, in the distal region, this relationship no longer holds (Fig. 5f). Previous work by other groups has considered circumferential stresses in the vessel wall averaged over the vessel cross-section for both stented and non-stented regions over a range of final diameters[5] whilst the aim of the current study is to consider the variation in the biological response within a single vessel at the level of individual struts. In this situation, the variations in circumferential stress observed are relatively small in comparison to the compressive stress, and for this reason, the force generated by strut contact is reported since this is less likely to be influenced by the accuracy of the segmented micro-CT data used to describe the stent geometry than the stress local to each strut. The reporting of force over a local region also reduces possible inconsistency in axial location between the numerical model and the processed histological section.

The CFD simulations indicate correlations between low values of *WSS* (<0.4 Pa), high *OSI* (>0.2) and greater neointimal growth (Figs. 5 and 6). The use of a physiological vessel curvature results in skewing of the velocity profile towards the upper region of the vessel and the formation of a recirculation zone within the proximal region of the domain, resulting in low values of *WSS* (Fig. 4, lower pane) which may influence localisation of ISR. These findings are consistent with those of other studies which indicate that lower shear stress is observed along the endocardial aspect of a curved coronary artery.[25] Such flow features have been linked to increases in both platelet and inflammatory cell activation.[11,22] The correspondence between these flow features and the area of greatest ISR in this porcine model supports the importance of this phenomenon. However, it is clear from Fig. 6 that the relationship between individual measures of fluid dynamics and the

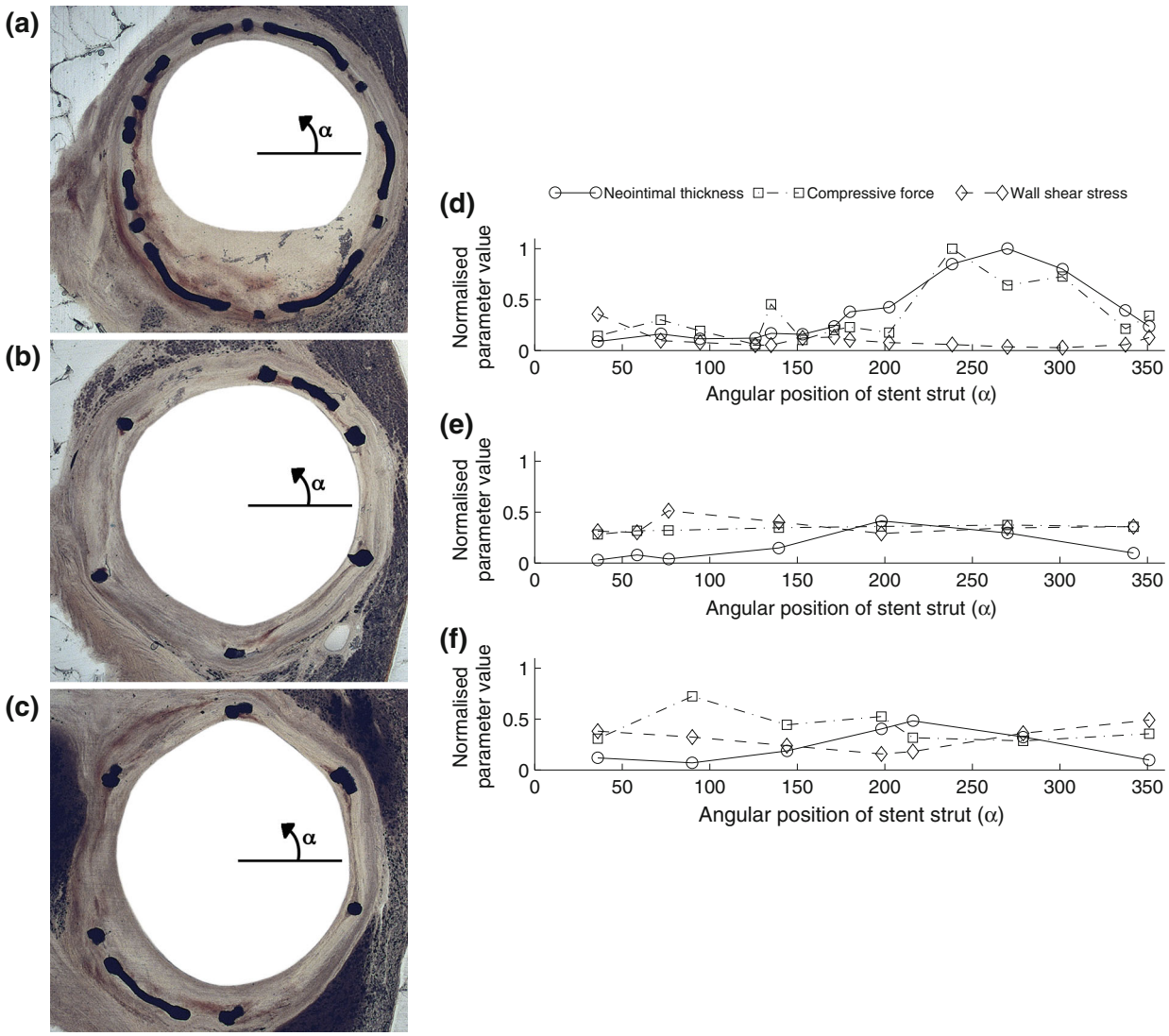

FIGURE 5. Comparison between histology and simulation results for three histology locations. (a, b, c) Histology sections from location 1, 4 and 7 respectively, representing the proximal, middle and distal regions of the stented vessel. The reference location for calculation of stent strut angle is shown where the solid line represents 0°. (d, e, f) Normalised variation of *NIT* (measured from histology), time-averaged *WSS* (computed from CFD) and *CF* (computed from FEM) with stent strut angle for the histology sections shown in (a, b, c). Values are normalised relative to the maximum value of each parameter over the whole stented region.

biological response is not consistent throughout the stented region.

Each of the individual stimuli considered in this study demonstrate a greater correlation with *NIT* in the proximal region of the stented vessel, where the neointimal thickening is most significant. However, correlation with individual parameters is not maintained along the length of the stent. Higher correlation is observed when considering parameters which include both a structural and fluid mechanics component, as shown in Fig. 6 and demonstrated in Table 1. These results are reported for comparison with data reported by other authors[5] and our findings are in agreement with Chen *et al.*, suggesting that both forms of mechanical stimuli play a role in determining the magnitude of the biological response.

Whilst computational studies are becoming increasingly sophisticated, with the use of patient-specific images for construction of the structural and/or fluid domains, the relative roles of solid and fluid mechanics in the biological process of ISR remains unresolved. Morlacchi *et al.*[34] included both structural simulations of the stent implantation and subsequent fluid dynamic simulations in the same domain. This representation was valuable for computational investigation of the influence of stent geometry under immediate post-implant conditions, but lacked direct representation of *in vivo* stent geometry and comparison

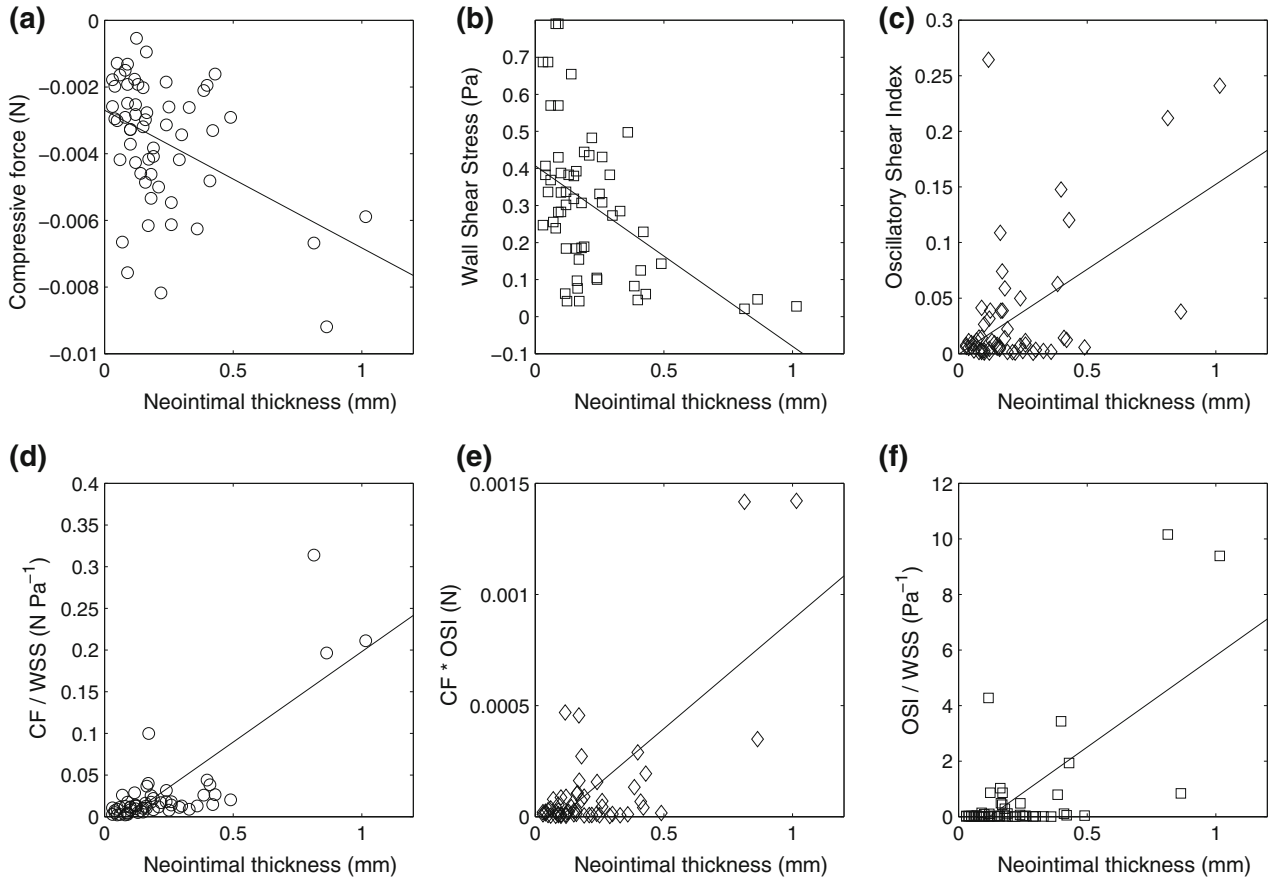

FIGURE 6. Relationship between computed parameters and *NIT* measured from histology for all 53 discrete strut locations. *NIT* is the horizontal axis for all plots. The vertical axis is used to plot the following primary parameters; (a) *CF* value computed from FEM (N). (b) Time-averaged *WSS* computed from CFD (Pa). (c) *OSI* computed from CFD (dimensionless). The following combined parameters are also plotted; (d) *CF* / *WSS* (N Pa^{-1}). (e) *CF* * *OSI* (N). (f) *OSI* / *WSS* (Pa^{-1}). The linear regression line is shown for each plot, for which the parameters are reported in Table 1.

TABLE 1. Regression parameters for plots shown in Fig. 6.

	CF (N)	*WSS* (Pa)	*OSI* (%)	*CF*/*WSS*	*CF***OSI*	*OSI*/*WSS*
m	0.004	−0.53	0.15	0.22	0.001	6.58
b	0.003	0.44	0.001	−0.02	−9e−5	−0.79
R^2	0.19	0.25	0.28	0.64	0.52	0.47

with histology to aid interpretation of the outcome. Sanmartín *et al.*[36] used a patient-specific representation of the vessel lumen, and found a similar negative correlation between *WSS* and *NIT*. However, detail regarding the influence of stent geometry was not directly reported. Chen *et al.*[5] reported correspondence between *in vivo* neointimal growth, fluid (*WSS*, *WSS* gradient, *OSI*) and mechanical (circumferential stress) stimuli as a function of axial location along the stent. However, the numerical model used an idealised deployed stent and parameters were averaged over each cross-section for comparison with the biological response at the level of each cross-section, rather than the level of each strut.

Here we use the vessel geometry immediately post-implant to evaluate hypotheses related to the progression of early-stage ISR. The methods employed within this paper account for the fact that not all struts at a particular axial location are subjected to identical conditions. The use of *in vivo* 3D micro-CT stent geometry captures such variation in stimuli between struts and the resulting correlation with local biological response. Further work will be required to evaluate the consistency of these correlations within porcine restenosis models and whether these effects are observed in a clinical context. The choice of a 14 day timepoint ensures that the magnitude of the biological response is sufficient to determine variations in

response at different regions of the vessel, whilst reducing the possibility that this response is dominated by later remodeling effects. At later timepoints it is possible that the solid mechanics and fluid dynamics within the stented artery will no longer be captured adequately by models based on the immediate post-deployment geometry. Models which are able to capture the growth of the new tissue allow computation of the fluid dynamics throughout the process of neointimal formation. Previous studies have proposed ISR growth models based on structural stimuli alone[24] and changes in fluid dynamic stimuli resulting from cellular proliferation.[42] Understanding of the coupling between cellular proliferation and the vascular stress state is currently limited, the use of more detailed models for the vascular wall incorporating the influence of the neointimal growth and the evolution of vascular wall stress following stent implantation may provide more detail of the relationship between vascular wall mechanics and progression of ISR.

Model Limitations

This study was based on data from a single stent deployed in a single animal and it is possible that the correlations reported here may vary between animals. However, the strength of the method described is that it enables the influence of stimuli to be investigated at the level of individual stent struts, enhancing the value of data available from a single experiment. The outcomes from this study could be used to guide future design of animal studies to consider the ISR response at different levels of injury and over different timepoints after implantation. An isotropic material description was used for the arterial wall in this study. This could be improved using a layer-specific representation for arterial tissue as reported by other authors.[10] However, it is anticipated that changes in material properties through the thickness of the arterial wall would have greater influence on the distribution of stress through the wall than the relative distribution of stress around the circumference of the vessel wall which determines the correlation between mechanical stimuli and biological response in this study. Whilst other studies have simulated the complete process of stent deployment the focus of this study was to consider stresses in a sample-specific case where both 3D stent geometry (from micro-CT) and biological response data (from histology) were available using the 3D micro-CT geometry of the stent to define a rigid contact surface, neglecting the stress-state in the stent.

The methods described provide insight into the relative role of three biomechanical factors in the initiation of ISR. The methodology relies on the ability to relate 2D histological data to 3D micro-CT data of the deployed stent. At the present time this is carried out manually. Development of novel imaging methods to provide both the 3D deployed stent geometry and the volumetric distribution of neointima would improve this process and Optical Projection Tomography is a potential candidate method to provide such data.[39] Fluid-structure analysis would be the most accurate approach to consider the detail of the coupling between fluid and solid effects. This would require a more detailed problem specification in order to incorporate appropriate solid mechanics boundary conditions.

CONCLUSION

This computational study considers the structural and fluid dynamic stimuli acting on a stented coronary artery in the post-deployment configuration using a combined FEM and CFD approach. The availability of corresponding histological data provides insight into the relationship between these factors and the degree of NIH. The results support the combined role of both structural and fluid mechanics to determine the magnitude of ISR at the level of individual struts. Extension of the methodology to consider the changes in structural and fluid stimuli during the development of NIH could provide insight into dynamic changes in these stimuli during the growth of neointimal tissue.

ACKNOWLEDGMENTS

We gratefully acknowledge financial support from the EU in the form of a Marie Curie fellowship (Project MeDDiCA Marie Curie Initial Training Network, www.meddica.eu, EU-FP7/2007-2013 under Grant agreement PITN-GA-2008-238113).

CONFLICT OF INTEREST

Brandis Keller, Claudia Amatruda, D Rodney Hose, Julian Gunn, Patricia Lawford, Gabriele Dubini, Francesco Migliavacca and Andrew Narracott declare that they have no conflict of interest.

ETHICAL STANDARDS

All institutional and national guidelines for the care and use of laboratory animals were followed and approved by the appropriate institutional committees. The work reported in this manuscript does not involve Human Subjects.

REFERENCES

[1]Bennett, M. R. In-stent stenosis: pathology and implications for the development of drug eluting stents. *Heart* 89(2):218–224, 2003.

[2]Boyle, C. J., A. B. Lennon, and P. J. Prendergast. Application of a mechanobiological simulation technique to stents used clinically. *J. Biomech.* 46(5):918–924, 2013.

[3]Boyle, C. J., *et al.* Computational simulation methodologies for mechanobiological modelling: a cell-centred approach to neointima development in stents. *Philos. Trans. R. Soc. A* 2010(368):2919–2935, 1921.

[4]Chaabane, C., *et al.* Biological responses in stented arteries. *Cardiovasc. Res.* 99(2):353–363, 2013.

[5]Chen, H. Y., *et al.* Mis-sizing of stent promotes intimal hyperplasia: impact of endothelial shear and intramural stress. *Am. J. Physiol. Heart Circ. Physiol.* 301(6):H2254–H2263, 2011.

[6]Chiastra, C., *et al.* Computational fluid dynamics of stented coronary bifurcations studied with a hybrid discretization method. *Eur. J. Mech. B* 35:76–84, 2012.

[7]Chiu, J–. J., and S. Chien. Effects of disturbed flow on vascular endothelium: pathophysiological basis and clinical perspectives. *Physiol. Rev.* 91(1):327–387, 2011.

[8]Chiu, J–. J., *et al.* A model for studying the effect of shear stress on interactions between vascular endothelial cells and smooth muscle cells. *J. Biomech.* 37(4):531–539, 2004.

[9]Colombo, A., *et al.* Cyclic strain amplitude dictates the growth response of vascular smooth muscle cells *in vitro*: role in in-stent restenosis and inhibition with a sirolimus drug-eluting stent. *Biomech. Model. Mechanobiol.* 212(4):671–683, 2013.

[10]Conway, C., *et al.* A computational test-bed to assess coronary stent implantation mechanics using a population-specific approach. *Cardiovasc. Eng. Technol.* 3(4):374–387, 2012.

[11]Duraiswamy, N., *et al.* Spatial distribution of platelet deposition in stented arterial models under physiologic flow. *Ann. Biomed. Eng.* 33(12):1767–1777, 2005.

[12]Edelman, E. R., and C. Rogers. Pathobiologic responses to stenting. *Am. J. Cardiol.* 81(7, Supplement 1):4E–6E, 1998.

[13]Gijsen, F. J., *et al.* Simulation of stent deployment in a realistic human coronary artery. *BioMed. Eng. OnLine* 7(23):1–11, 2008.

[14]Gogas, B. D., *et al.* The edge vascular response following implantation of the absorb everolimus-eluting bioresorbable vascular scaffold and the XIENCE V metallic everolimus-eluting stent. First serial follow-up assessment at six months and two years: insights from the first-in-man ABSORB Cohort B and SPIRIT II trials. *EuroIntervention* 9(6):709–720, 2013.

[15]Gojova, A., and A. I. Barakat. Vascular endothelial wound closure under shear stress: role of membrane fluidity and flow-sensitive ion channels. *J. Appl. Physiol.* 98(6):2355–2362, 2005.

[16]Gunn, J., *et al.* Coronary artery stretch versus deep injury in the development of in-stent neointima. *Heart* 88(4):401–405, 2002.

[17]Huo, Y., *et al.* Effects of vessel compliance on flow pattern in porcine epicardial right coronary arterial tree. *J. Biomech.* 42(5):594–602, 2009.

[18]Kleinstreuer, C., *et al.* Hemodynamic parameters and early intimal thickening in branching blood vessels. *Crit. Rev. Biomed. Eng.* 29(1):1–64, 2001.

[19]Kleinstreuer, C., *et al.* Hemodynamic parameters and early intimal thickening in branching blood vessels. *Crit. Rev. Biomed. Eng.* 29(1):1–64, 2001.

[20]Kolandavel, M., *et al.* The effects of time varying curvature on species transport in coronary arteries. *Ann. Biomed. Eng.* 34(12):1820–1832, 2006.

[21]Koskinas, K. C., *et al.* Role of endothelial shear stress in stent restenosis and thrombosis: pathophysiologic mechanisms and implications for clinical translation. *J. Am. Coll. Cardiol.* 59(15):1337–1349, 2012.

[22]Kroll, M., *et al.* Platelets and shear stess. *Blood* 88(5):1525–1541, 1996.

[23]LaDisa, J. F., *et al.* Stent implantation alters coronary artery hemodynamics and wall shear stress during maximal vasodilation. *J. Appl. Physiol.* 93(6):1939–1946, 2002.

[24]LaDisa, Jr., J. F., *et al.* Alterations in wall shear stress predict sites of neointimal hyperplasia after stent implantation in rabbit iliac arteries. *Am. J. Physiol. Heart Circ. Physiol.* 288(5):H2465–H2475, 2005.

[25]LaDisa, J. F., *et al.* Alterations in regional vascular geometry produced by theoretical stent implantation influence distributions of wall shear stress: analysis of a curved coronary artery using 3D computational fluid dynamics modeling. *BioMed. Eng. OnLine* 5(40):11, 2006.

[26]Linder-Ganz, E., *et al.* Pressure–time cell death threshold for albino rat skeletal muscles as related to pressure sore biomechanics. *J. Biomech.* 39(14):2725–2732, 2006.

[27]Malek, A. M., S. L. Alper, and S. Izumo. Hemodynamic shear stress and its role in atherosclerosis. *JAMA* 282(21):2035–2042, 1999.

[28]Malek, A., and S. Izumo. Physiological fluid shear stress causes downregulation of endothelin-1 mRNA in bovine aortic endothelium. *Am. J. Physiol. Cell Physiol.* 263(2):C389–C396, 1992.

[29]Messenger, J., *et al.* 3D coronary reconstruction from routine single-plane coronary angiograms: clinical validation and quantitative analysis of the right coronary artery in 100 patients. *Int. J. Card. Imaging* 16(6):413–427, 2000.

[30]Moazzam, F., *et al.* The leukocyte response to fluid stress. *Proc. Natl. Acad. Sci.* 94(10):5338–5343, 1997.

[31]Moore, Jr., J., and J. L. Berry. Fluid and solid mechanical implications of vascular stenting. *Ann. Biomed. Eng.* 30(4):498–508, 2002.

[32]Morlacchi, S., *et al.* Sequential structural and fluid dynamic numerical simulations of a stented bifurcated coronary artery. *J. Biomech. Eng.* 133(12):1–11, 2011.

[33]Morlacchi, S., *et al.* Hemodynamics and in-stent restenosis: micro-CT images, histology, and computer simulations. *Ann. Biomed. Eng.* 39(10):2615–2626, 2011.

[34]Murphy, J., and F. Boyle. Predicting neointimal hyperplasia in stented arteries using time-dependant computational fluid dynamics: a review. *Comput. Biol. Med.* 40(4):408–418, 2010.

[35]Nichols, W. W., and M. F. O'Rourke. McDonald's blood flow in arteries (3rd ed.). Philadelphia: Lea & Febiger, 1990.

[36]Sanmartín, M., *et al.* Influence of shear stress on in-stent restenosis: *in vivo* study using 3D reconstruction and computational fluid dynamics. *Revista Española de Cardiología* 59(1):20–27, 2006.

[37]Selvarasu, N. K. C., and D. K. Tafti. Investigation of the effects of dynamic change in curvature and torsion on pulsatile flow in a helical tube. *J. Biomech. Eng.* 134(7):071005–071017, 2012.

[38]Seo, T., L. G. Schachter, and A. I. Barakat. Computational study of fluid mechanical disturbance induced by endovascular stents. *Ann. Biomed. Eng.* 33(4):444–456, 2005.
[39]Sharpe, J., *et al*. Optical projection tomography as a tool for 3D microscopy and gene expression studies. *Science* 296(5567):541–545, 2002.
[40]Stefanini, G. G., and D. R. Holmes, Jr. Drug-eluting coronary-artery stents. *N. Engl. J. Med.* 368(3):254–265, 2013.
[41]Stettler, C., *et al*. Outcomes associated with drug-eluting and bare-metal stents: a collaborative network meta-analysis. *Lancet* 370(9591):937–948, 2007.
[42]Tahir, H., *et al*. Multi-scale simulations of the dynamics of in-stent restenosis: impact of stent deployment and design. *Interface Focus* 1(3):365–373, 2011.
[43]Thury, A., *et al*. Focal in-stent restenosis near step-up. *Circulation* 105(23):e185–e187, 2002.
[44]Timmins, L. H., *et al*. Increased artery wall stress post-stenting leads to greater intimal thickening. *Lab. Investig.* 91(6):955–967, 2011.
[45]Wang, J., and B. Thampatty. An introductory review of cell mechanobiology. *Biomech. Model. Mechanobiol.* 5(1):1–16, 2006.